An experimental system to acquire aeroacoustic properties on wind turbine blades

An experimental system to acquire aeroacoustic properties on wind turbine blades

J Deparday[1], H Müller[2], T Polonelli[2] and S Barber[1]

[1]Institute for Energy Technology, OST - Eastern Switzerland University of Applied Sciences, Oberseestrasse 10, CH-8640 Rapperswil-Jona.
[2]Center for Project Based Learning, D-ITET, ETH Zürich, Gloriastrasse 35, CH-8092 Zürich

E-mail: julien.deparday@ost.ch

Abstract. Wind turbine noise is a key issue preventing the successful exploitation of the full potential of wind energy throughout the world, especially in urban areas. To better assess and predict wind turbine noise, several aeroacoustic simulations and models have been developed over the past. Many semi-empirical models for noise emission and propagation rely on aeroacoustic properties at the blade level, including the pressure gradient, the spectrum of the pressure fluctuations, the convection velocity and the coherence lengths. Field measurements of these local quantities on operating wind turbines are valuable to improve the accuracy of the models. In the Aerosense project, a cost-effective smart measurement system is being developed that is thin, easy to install without damaging the blade, low power, self-sustaining and wirelessly transmitting. This measurement system uses MEMS sensors, which require some calibrations and corrections to obtain sufficiently accurate data. This paper describes the experimental system and its workflow, which has been developed within the Aerosense project to obtain sufficiently accurate measurements for semi-empirical noise emission and propagation models. The experimental system and its workflow are then validated in an anechoic wind tunnel on a NACA63-418 airfoil. The results show that this experimental system is able to acquire relevant aeroacoustic properties on operating wind turbines.

1. Introduction

Close to urban areas, wind turbines have to shut down when their expected noise level at a few hundred meters away from the wind turbines is higher than a certain limit set by the regulations, which vary from country to country. More accurate simulations of the noise emission and propagation from the wind turbine blades would help to better estimate the noise level and to reduce the shut-down period, thus increasing the revenues of wind farm owners/operators. Noise propagation models [1] and aeroacoustic semi-empirical models for noise emission [2, 3] require local blade aerodynamic pressure distribution as well as statistical parameters, such as convection velocity and coherence lengths. However, compared to research based on numerical simulations, there are very few published measurements on rotor blades due to the complexity of installation and the use of the measurement system. Such measurements are still challenging, often requiring custom-made rotor blades with embedded sensors [4, 5, 6, 7].

Recent developments in electronics, wireless communication, and micro-electro-mechanical systems (MEMS) sensors are making it possible to acquire data in a cost-effective and energy efficient way [8]. Therefore, a smart measurement system that is thin, easy to install without damaging the blade, low power, self-sustaining and wirelessly transmitting is being developed

in the Aerosense project [9]. One of the main objectives of the Aerosense project is to develop a MEMS-based surface pressure and acoustic smart measurement system, which can easily be installed on any wind turbine. For that purpose, MEMS sensors are promising candidates as they are easily available on the market. They are a cost-effective, small and low power alternative compared to high-cost and high quality sensors that are often bulky. However, MEMS microphones also come with a lower sensitivity and frequency ranges, which tend to reduce the precision of the measurements with respect to top-of-the-range sensors. Selected MEMS pressure sensors, required to measure the pressure gradient for aeroacoustic models, have an accuracy of about 100 Pa while top-of-the-range pressure scanners can reach an accuracy of less than 5 Pa. However, we found no quantitative comparison between aeroacoustics data from MEMS and state-of-the-art sensors in wind turbine aerodynamics. Therefore, we defined a complete experimental system and workflow for the collection and post-processing of aeroacoustic data in order to obtain aeroacoustic characteristics with sufficient accuracy for semi-empirical models.

In section 2, the Aerosense system and its components are first presented, followed by a description of the experimental system and workflow. A demonstration of part of the workflow is described in section 3, where measurements from MEMS sensors are compared with measurements from top-of-the-range microphones and pressure scanner.

2. Experimental system and workflow description

The Aerosense system is split into three main sub-systems: (1) the sensor nodes on the blades, which measure the pressure distribution along the chord, the high-frequency pressure fluctuations at the trailing edge, the gradient of pressure at the leading edge and the relative position of the blade using an Inertial Measurement Unit (IMU), and sends the data wirelessly to the base station; (2) the base station at the foot of the wind turbine, which collects measurements from all sensor nodes together with the atmospheric pressure and temperature and sends the data to the cloud-based storage; (3) the on-cloud digital twin, which collects the data from the base station and processes the in-field measurements, automatically analyses them, and uses them to compare or improve low and high-fidelity simulations in order to create values for the customers. The workflow developed in the present work concerns optimising the accuracy of MEMS-based aerodynamic and acoustic measurements and obtaining statistical parameters in order to build semi-empirical models and ultimately provide added value to customers. The combination of the different sensors on the sensor nodes is used to improve the quality of the sensors as shown in figure 1 and discussed in the next sections.

2.1. Inertial measurement unit

For the IMU measurements, the workflow involves the steps shown in the top row of figure 1. The nine-axis IMU combines an accelerometer, gyroscope and magnetometer. It infers the azimuth position of the blade, as well as the rotational velocity and the accelerations encountered by the sensor node. We use the Madgwick filter[10] to estimate the position of the sensor node. This algorithm is known to be efficient and to work well with and without the magnetometer, as the measurements from the magnetometer might be greatly disturbed by the large magnetic field surrounding the wind turbine. Accelerations, rotational speed and blade position are valuable by themselves and are also used to calibrate the pressure measurements from the barometers.

2.2. Pressure measurements

For the pressure measurements, the workflow involves the steps shown in the second row of figure 1. A total of 40 LPS27HHW barometers, from STMicroelectronics, are distributed along the chord to measure the pressure distribution on the blades. The sensors are watertight and less than 2 mm thick. The barometers also possess a temperature sensor to compensate the main temperature fluctuations. Unlike pressure measurement systems installed in previous

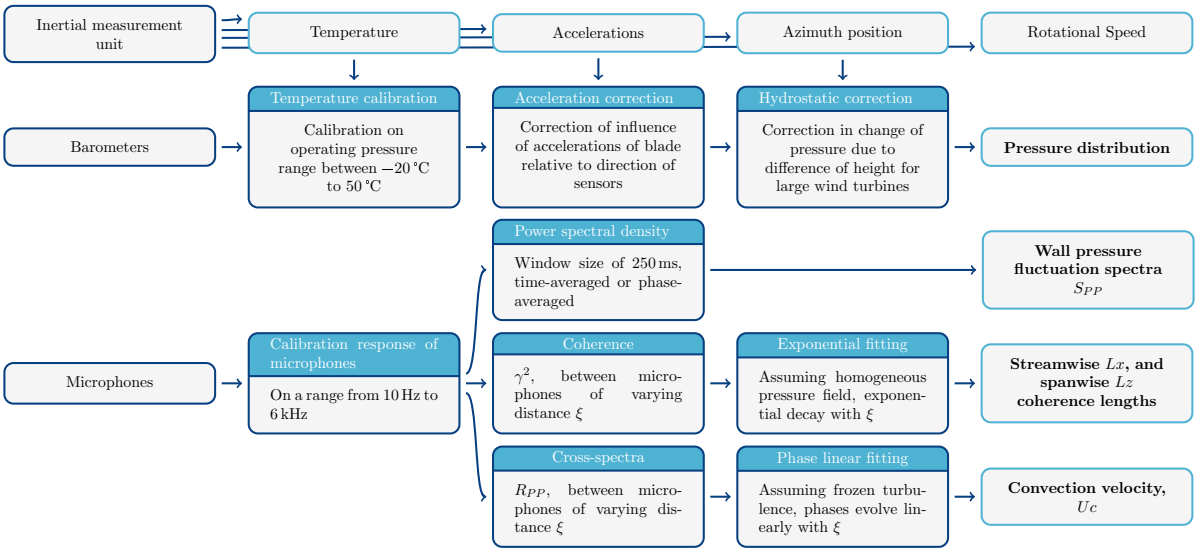

Figure 1: Workflow to improve the quality of measurements from MEMS sensors and acquire the statistical properties needed for aeroacoustic models.

experimental campaigns [4, 6, 7], MEMS barometers do not need a reference pressure, which can be cumbersome to acquire on rotating machines. However they also need corrections, some of them similar to those of previous campaigns (e.g. [4]), including hydrostatic, centrifugal acceleration corrections.

According to the manufacturer, the absolute accuracy of the barometers is 100 Pa. However, the dynamic pressure on multi-megawatt wind turbine is at least in the order of 1000 Pa, and an error of less than of 1% would require an accuracy in the order of tens of Pascals. As the temperature on an operating wind turbine blade may vary significantly in the full working range of the barometers and can affect their accuracy, the workflow involves specifically calibrating them for a pressure range from 800 hPa to 1100 hPa and for a temperature range from −20 °C to 50 °C in a dedicated calibration chamber. For each barometer, a second-order polynomial surface fitting is applied on their temperature and pressure measurements.

In addition, the barometer values depend on the acceleration and need to be calibrated to take into account the accelerations of the blade. When a barometer sensor is placed upside-down, an average pressure difference of 5 Pa is read, due to a 2g difference on the sensor. On multi-megawatt wind turbines, the acceleration can reach 100 m s^{-2} which would affect the sensor measurement by 50 Pa. The influence of the acceleration is taken into account based on the normal direction of the barometers relative to the direction of the acceleration measured by the accelerometer of the IMU.

For very large wind turbines, another correction takes into account the change of pressure due to the difference of height depending on the azimuth position of the blades. On multi-megawatt wind turbines, an Aerosense sensor node on the tip of the blade can have a difference of elevation of more than 100 m during one rotation. This difference of height affects the pressure measurement by about 1000 Pa, which is the order of magnitude of the dynamic pressure on the blade. The pressure difference due to change of height of the sensor node is estimated by a linear regression of the pressure according to the elevation. The difference of pressure is corrected based on the azimuth position measured by the IMU and the position of the sensor node on the blade.

After these calibrations and corrections, the barometers do not provide the pressures relative

to a static pressure as it is commonly used. The pressure measured by the barometer is the atmospheric pressure and the variations of pressure due to the presence of the wind turbine blade. The variations of the atmospheric pressure need to be detected and removed from the measurements. They have lower dynamics than the variations due to the wind turbine blade, and are measured by a barometer in the base station, at the foot of the tower, protected from the wind. Theoretically, at a unique radial position on the blade, the atmospheric pressure should be the same for all barometers, however the pressure is relative to vacuum which might slightly leak and yields to an undetermined long-term drift of about 1 hPa/year. A "zeroing" of the barometers is therefore required when possible to obtain a sufficient accuracy. This process must be done when there is no wind. While it is simple in a wind tunnel, it is not that trivial on a wind turbine. The zeroing process is automatically done when the recorded acceleration and rotational speed, as well as the standard deviation of the pressure are lower than specific thresholds, depending on the type of the wind turbine.

After these steps to correct and improve the average pressure measurements, we can calculate the pressure gradient around the blade, which is one of the inputs for aeroacoustic models.

2.3. Pressure fluctuation measurements

For the pressure fluctuation measurements, the workflow involved the steps shown in the bottom row of figure 1. The pressure fluctuation frequencies of interest for noise propagation are between 100 Hz to 5000 Hz. For the Aerosense measurement system, we chose the microphones Vesper VM2020, which are dust resistant, have a thickness of less than 2 mm, and have a high acoustic overload point of 152 dB. The sampling frequency supported by our system is 16 kHz. The generated noise by rotor blades mostly comes from the pressure fluctuation near the trailing edge on the suction side [11], if we neglect inflow turbulent noise and tip noise. The microphones are placed in a "L" shape as close as possible to the trailing edge, with varying distance between the sensors in order to assess the streamwise and spanwise coherence lengths as well as the pressure fluctuations and the convection velocity [12, 13], which are required for semi-empirical and analytical aeroacoustic models.

In the Aerosense measurement system, the microphones are embedded in a housing, creating a small cavity above the microphones which might affect the response of the microphones. A calibration is therefore applied on the microphones using a loudspeaker and a reference microphone as explained in [14, 13]. After this step made to improve the accuracy of the pressure fluctuations measurements, we can retrieve the statistical parameters of interest for aeroacoustic models using the array of microphones positioned on the trailing edge of the blade.

The pressure frequency fluctuations spectrum is computed using the power spectrum density S_{pp} with rectangular windows of 250 ms, which can be time-averaged or phase-averaged (according to azimuth position of the blade) depending on the purpose. The results of our measurement system in an anechoic wind tunnel are presented in section 3.

The cross-spectra R_{pp} and the resulting coherence γ^2 between the microphones provide the statistical parameters required for semi-empirical models: the coherence lengths and the convection velocity. The coherence length is a statistical value describing the sizes of the turbulent structures in the spanwise and chordwise directions. The convection velocity quantifies the speed of convection of these turbulent structures in the chordwise direction. The coherence γ^2, between two signals shows how similar they are:

$$\gamma^2(\xi,\omega) = \frac{|R_{pp}(\xi,\omega)|^2}{S_{pp}(x,\omega)S_{pp}(x+\xi,\omega)} \quad , \tag{1}$$

where $S_{pp}(x)$ is the spectrum of the microphones located at the position x. Assuming that the pressure field is homogeneous, based on Corco's model [15], the streamwise coherence function

γ is deduced from the expression:

$$\gamma^2(\xi,\omega) = exp\left(\frac{-|\xi|}{Lz}\right) \quad . \tag{2}$$

The chordwise and spanwise length scales, respectively Lx and Lz, are estimated by fitting the measured coherence functions by an exponential profile.

Cross-spectra are calculated for different distances between the microphones, $R_{PP}(\xi,\omega)$, where ω is the angular frequency, and ξ the distance between microphones. As the distance between microphones varies and is not linear, the amount of ξ values are greater than the amount of sensors. Assuming the turbulence is frozen between two points of measurements, the phase, Φ of the cross-spectra is linked to the convection velocity U_c:

$$\Phi = \frac{\omega\xi}{U_c}. \tag{3}$$

Two methods can be applied to estimate the convection velocity: (1) temporally with ω, using two microphones with a high coherence (above 0.8) on the full frequency range; or (2) spatially with ξ, using all microphones. The phase should be linear with the distance between the microphones, and a linear fitting would provide the convection velocity. We test and compare these two methods in the next section.

3. Demonstration of the workflow

3.1. Experimental set-up

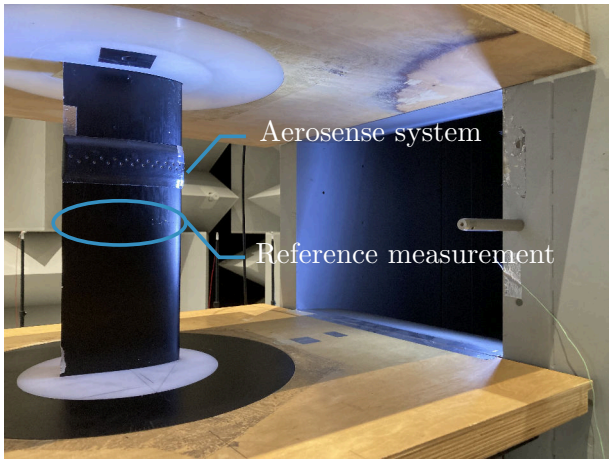

Figure 2: Position of the Aerosense measurement strip with 40 barometers inserted in a flexible 3D-printed housing above the reference pressure measurement at mid-span on a NACA63-418.

The workflow was demonstrated in the anechoic wind tunnel at Ecole Centrale de Lyon. The main goal of this measurement campaign was to quantify the accuracy and reliability of the MEMS sensors used in the Aerosense measurement system compared with high-quality reference measurements. A NACA 63418 wing profile with a chord of 12 cm and a span of 30 cm was placed between two end-plates at the outlet of the open-jet wind tunnel of 0.4 m x 0.3 m. Measurements were carried out for different wind speeds (from 12.5 m s^{-1} to 50 m s^{-1}, $Re = 1 \times 10^5$ to 6.5×10^5, $Ma = 0.04$ to 0.22) and for different inflow turbulent intensity: 0% as a reference case and 8% to represent field measurements. The Aerosense measurement system was tested for static angles of attack from $-4°$ to $24°$. The barometers of the Aerosense measurement system were compared with 20 pressure points measured at mid-span using a Kulite KMPS-1-64 pressure scanner (figure 2). The pressure scanner acquired pressure data from pressure orifices via capillary tubes at a sampling frequency of 1.1 kHz. The microphones of the Aerosense measurement

system were compared with 12 Brüel & Kjaer 4958 type microphones distributed along the chord, using the same pressure orifices (figure 3). The acquired fluctuating wall pressure signals recorded at 51.2 kHz were calibrated as explained in the previous section 2.3. The positions of the pressure orifices are the same as presented in [16]. Measurements with GRAS 48LX-4 UTP microphones stuck at the trailing edge of the blade were also carried out (figure 4). These high-quality microphones have a thickness of about 2 mm, similar to the Aerosense measurement system and should influence the pressure fluctuation measurements similarly to the Aerosense microphones.

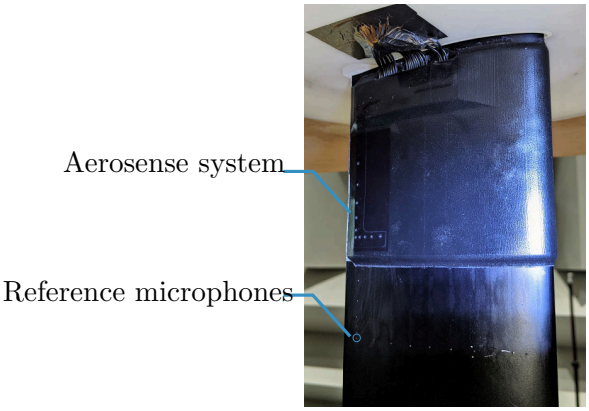

Figure 3: Position of the Aerosense measurement strip with 10 microphones positioned in a "L-shape", inserted in a flexible 3D-printed housing glued above the reference measurement system at mid-span.

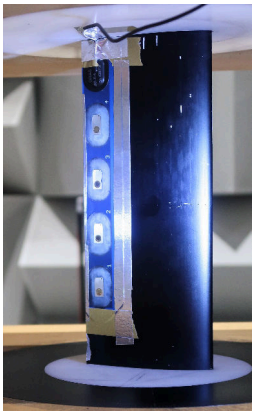

Figure 4: Position of high-quality microphones GRAS 48LX-4 UTP at 15 mm from the trailing edge, with a thickness similar to the Aerosense system.

3.2. Pressure distribution

For the Aerosense measurements, 40 barometers were integrated within a housing made of a smooth and flexible polyjet 3D-print, on which a leading-edge protection foil was glued to be able to easily install and remove the sensor strip (figure 2). The bottom of the housing was placed 35 mm above the pressure orifices that are located at mid-span. The total thickness of the housing is 2.8 mm, which corresponds to 2.5% of the chord, but is also as large as the leading edge radius. Due to the very small curvature radius of the leading edge, the Aerosense measurement system had to endure too much stress, and two of the sensors at the leading edge broke. The other sensors worked properly for all measurement points.

The tested barometer strip has been calibrated at EMPA, the Swiss Federal Laboratories for Materials Science and Technology, during 36 hours to record about 30 000 measurement points at different pressures and temperatures. Based on our calibration dataset, from a root-mean-squared error of 98 Pa, we reached after calibration an absolute accuracy of 11 Pa. The corrections for hydrostatic, acceleration do not need to be applied, but the zeroing of the barometers were made at the beginning and end of half days of measurements.

The resulting pressure distribution coefficients, $C_P = Pressure/(1/2\rho U_\infty^2)$, where ρ is the air density, are presented in figure 5 for the case at $U_\infty = 50\,\mathrm{m\,s^{-1}}$, with no turbulence grid, at different static angles of attack. The reference pressure measurements from the pressure orifices recorded by the Kulite pressure scanner are shown in comparison with the markers. The envelope comprising four standard deviations ($\pm 2\sigma$) for the 30 s measurement run is indicated with the shaded areas for the Aerosense measurements and with error bars for the reference

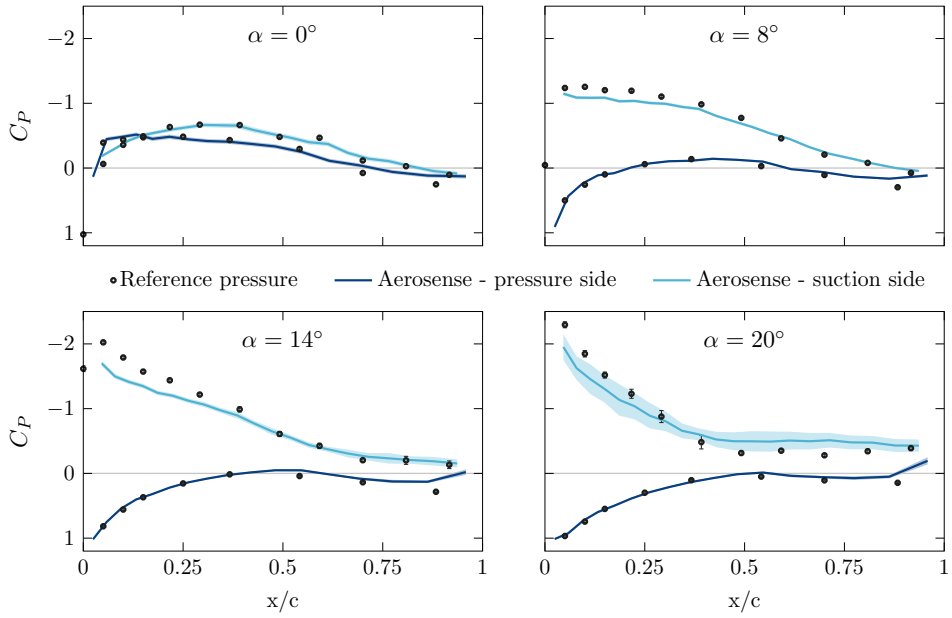

Figure 5: Average pressure coefficient distribution along the chord c for the Aerosense measurement system with barometers at $U_\infty = 50\,\mathrm{m\,s^{-1}}$ with no turbulence grid at four different angles of attack. The shaded areas for the Aerosense system and the error bars for the reference pressure show the variations during 30 s using ± 2 standard deviations.

pressures. As long as the flow is attached (below 20°), the fluctuations are very small. At 0°, on a non-symmetrical airfoil, the pressure and suction side are not the same as expected, and the Aerosense pressures correspond well to the reference pressures. When the angle of attack increases, the leading-edge suction is underestimated by the Aerosense system. This might be due to the thickness of the Aerosense system, which increased the radius at the leading edge but did not scale the chord length as the extremity of the system ended at the trailing edge. This will not be a problem on operating multi-MW wind turbines because the thickness of the Aerosense system will be no more than 2% of the maximum thickness of the blade section. The values on the pressure side were correctly measured by the Aerosense system. The plateau on the suction side near the trailing edge at 14° and 20°, measured by both pressure systems, is due to the separation of the flow at the trailing edge.

After calibration and corrections, the MEMS barometers measure accurately the dynamic pressure on an airfoil for all angles of attack, wind speed and turbulence intensity tested.

3.3. Wall pressure fluctuations at the trailing edge

For the Aerosense measurements, 10 microphones were installed at the trailing edge to measure the spectrum of the wall pressure fluctuations and to obtain the statistical parameters: convection velocity U_C and chordwise and spanwise coherence lengths, respectively Lx and Lz. The results shown below are for an incoming wind speed of $U_\infty = 50\,\mathrm{m\,s^{-1}}$, and with a turbulence intensity of 8%. This corresponds to the configuration the closest to what could be recorded in the field, and the turbulence ensures a transition to a turbulent boundary layer for both the Aerosense and reference measurements.

First a calibration of the Aerosense microphones has been applied. The Aerosense microphones detect correct amplitudes and frequencies until 4 kHz. Between 4 kHz to 8 kHz, the calibration compensates the underestimation of the amplitude of the pressure fluctuations

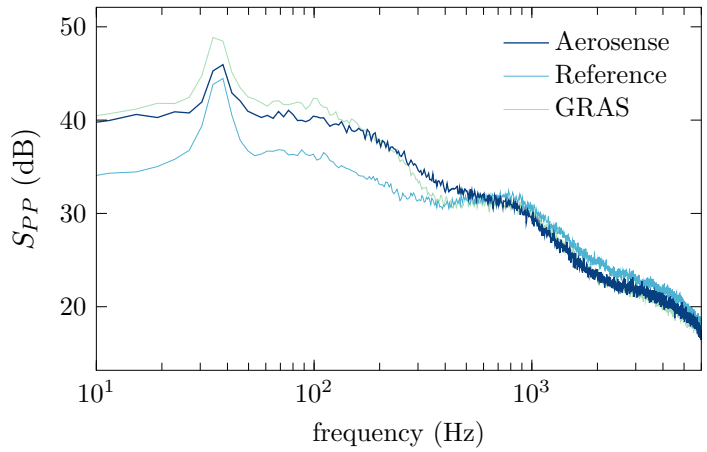

Figure 6: Power spectrum of pressure fluctuations at $U_\infty = 50\,\mathrm{m\,s^{-1}}$, $\alpha = 8°$ with an inflow turbulence intensity of 8% for a microphone at 10 mm from the trailing edge. Comparison with a flush reference microphone at the same distance from the trailing edge, and with an external GRAS microphone at 15 mm from the trailing edge but with a thickness similar to the Aerosense system.

by the Aerosense measurement system.

Figure 6 shows the power spectrum density S_{pp} for the microphone located at the corner of the "L", the closest to the trailing edge i.e. at 10 mm from the trailing edge, and is compared with the reference microphone at the same chordwise position and also with the external GRAS microphones, adding a thickness to the trailing edge similar to the Aerosense system. It can be seen that a peak at 40 Hz is captured by all sensors. Up to 300 Hz, the external sensors (Aerosense and GRAS microphones) record an amplitude of more than 5 dB with respect to the reference microphones. For frequencies above 500 Hz, the power decay is correctly measured by the Aerosense sensor node. The Aerosense system provide accurate wall pressure fluctuation spectra, and the thickness of the Aerosense measurement system of 3 mm will be negligible on a wind turbine blade where the chord length is two orders of magnitude higher.

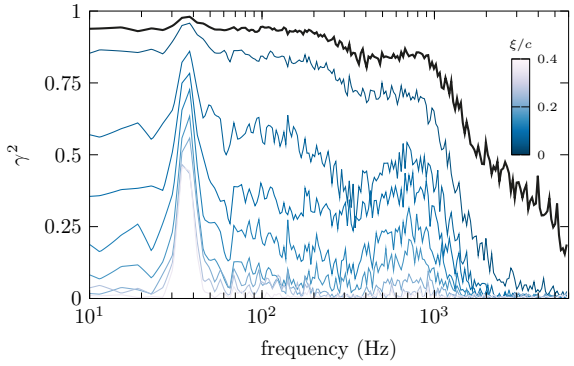

Figure 7: Coherence γ^2 between Aerosense microphones with a turbulence intensity of 8%, at $\alpha = 0°$ at $U_\infty = 50\,\mathrm{m\,s^{-1}}$. In black, the two closest microphones in the streamwise direction $\xi/c = 0.038$; in shades of blue, in the spanwise direction.

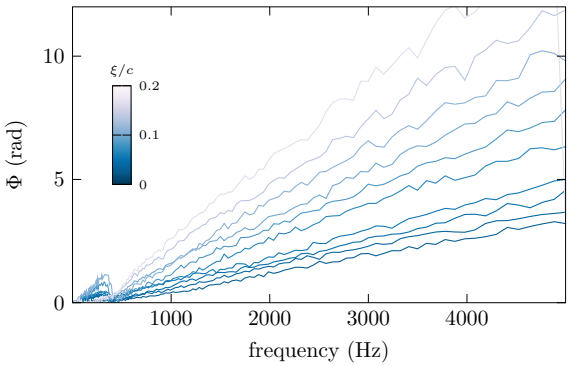

Figure 8: Phases Φ of the cross-spectrum R_{PP}, between the 5 Aerosense microphones in the streamwise direction for different distances ξ/c with a turbulence intensity of 8%, at $\alpha = 0°$ at $U_\infty = 50\,\mathrm{m\,s^{-1}}$.

The spanwise coherence, shown in shades of blue in figure 7, decreases when the distance between the microphones ξ/c is increased. The decay of the coherence level with respect to the distance seems to be exponential and confirms equation (2). The coherence between the sensor in the corner of the "L" and its closest microphone in the chordwise direction (in black

in figure 7) shows values above 0.8 at least until 1 kHz. This high value indicates it should be possible to calculate the convection velocity (equation (3)) using the temporal method.

Figure 8 shows the phases of the cross-spectra between the streamwise Aerosense microphones. For all distances between sensors, the phase increases linearly with the frequency; and for a fixed frequency, the slope of the phase increases with the distance. This suggests the convection velocity could also be estimated using the spatial method using the slope ϕ/ξ to calculate Uc.

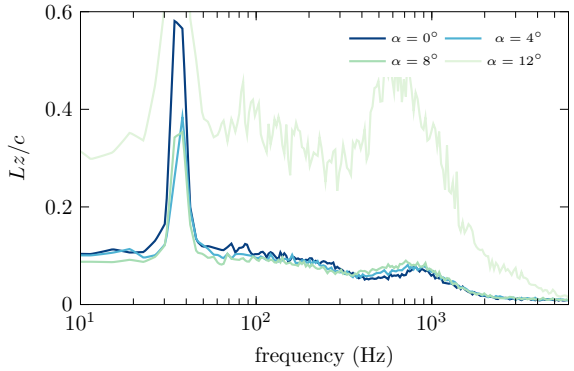

Figure 9: Spanwise coherence length Lz/c for different angles of attack with a turbulence intensity of 8%, at $U_\infty = 50\,\mathrm{m\,s^{-1}}$.

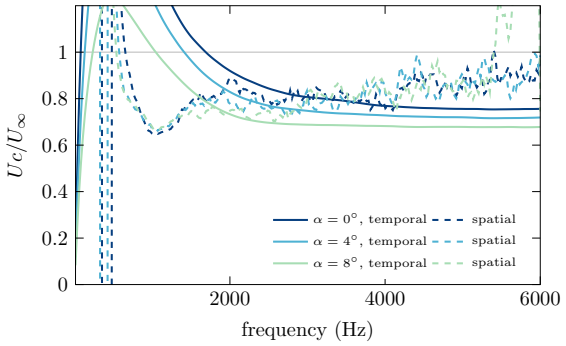

Figure 10: Convection velocity Uc/U_∞ for different angles of attack with a turbulence intensity of 8%, at $\alpha = 0°$ at $U_\infty = 50\,\mathrm{m\,s^{-1}}$.

Figure 9 shows the coherence lengths assuming an exponential decay with the distance (equation (2)). The coherence lengths have been scaled by the chord length, even though it is more standard to scale it with the thickness of the boundary layer δ, which we could not measure here. When the flow is attached in the trailing edge region (0° to 8°), the coherence length is the same for all angles of attack with a small decrease for frequencies higher than 1 kHz. Above 10°, the flow starts to detach at the trailing edge as seen by the plateau of pressure in figure 5, the estimated coherence length is at least three times higher. At the large peak at 40 Hz seen in the spectrum in figure 6, the coherence length reaches 50% of the chord length. This value seems too high and further analysis should be done to improve the coherence length computation.

Figure 10 shows the estimation of the convection velocity using the two methods mentioned in section 2: temporally using only two highly correlated microphones (in solid lines) or spatially with all microphones (in dashed lines). Below 1000 Hz, the values are much larger than the incoming wind speed, meaning the convection velocity is badly estimated. Above 1000 Hz, both methods show results with similar values between $0.6U_\infty$ and $0.8U_\infty$, which corresponds to what is found in the literature [2]. The temporal method indicates an increase in the convection velocity with the angle of attack. The spatial method indicates similar values for all angles of attack but a slight increase of the convection velocity with the frequency. These results are promising, further analysis should be done to improve the estimation of the convection velocity.

4. Conclusions

A MEMS-based cost-effective smart measurement system that is thin, easy to install without damaging the blade, low power, self-sustaining and wirelessly transmitting is being developed in the Aerosense project. In order to increase the measurement accuracy of the MEMS sensors, a specific experimental system and workflow were described in this paper. Precise calibration has been made to obtain the most of the sensors, and corrections fusing measurements from

accelerometers and gyrometers with barometers and microphones are computed to discard influence of accelerations, atmospheric pressure variations, temperatures, and hydrostatic pressure. To provide a comparison of aeroacoustic measurement between MEMS sensors and high-quality microphones, measurements were carried out in an anechoic wind tunnel. The results showed that the pressures and wall pressure fluctuations could be obtained to a suitable accuracy by the MEMS sensors of the Aerosense measurement system. These measurements also showed that the Aerosense measurement system could also provide the useful statistical parameters, coherence lengths and convection velocity for semi-empirical aeroacoustic models.

Acknowledgments

This work is funded by the BRIDGE Discovery Programme of the Swiss National Science Foundation and Innosuisse, project number $40B2-0\_187087$. We would like to thank in particular Pascal Souchotte and Emmanuel Jondeau for all the preparation and help during the experimental campaign, as well as Edouard Salze who also advised us together with Pascal and Emmanuel during the processing of the data.

References

[1] Barlas E, Zhu W J, Shen W Z, Dag K O and Moriarty P 2017 *The Journal of the Acoustical Society of America* **142** 3297–3310
[2] Bertagnolio F, Madsen H A, Fischer A and Bak C 2017 *Journal of Sound and Vibration* **387** 127–162
[3] Rozenberg Y, Robert G and Moreau S 2012 *AIAA Journal* **50** 2168–2179
[4] Medina P, Singh M, Johansen J, Rivera Jove A, Machefaux E, Fingersh L and Shreck S 2011 Aerodynamic and performance measurements on a swt-2.3-101 wind turbine *Windpower 2011* pp 1–11
[5] Troldborg N, Bak C, Madsen H A and Skrzypinski W Danaero mw ii: Final report Tech. Rep. DTUWind Energy E-0027 DTU Wind Energy
[6] Schepers J G and Schreck S J 2019 *Wiley Interdisciplinary Reviews: Energy and Environment* **8** e320
[7] Wu G, Zhang L and Yang K 2019 *Applied Sciences* **9** 482
[8] Fischer R, Mueller H, Polonelli T, Benini L and Magno M 2021 Windnode: A long-lasting and long-range bluetooth wireless sensor node for pressure and acoustic monitoring on wind turbines *4th IEEE International Conference on Industrial Cyber-Physical Systems (ICPS)*
[9] Barber S, Deparday J, Magno M, Polonelli T, Fischer R and Mueller H 2022 *Wind Energy Science Discussions* **2022** 1–16
[10] Madgwick S, Harrison A and Vaidyanathan R 2011 Estimation of imu and marg orientation using a gradient descent algorithm *2011 IEEE international conference on rehabilitation robotics* (IEEE) pp 1–7
[11] Oerlemans S 2011 Wind turbine noise: primary noise sources Tech. Rep. NLR-TP-2011-066 National Aerospace Laboratory NLR
[12] Salze E, Bailly C, Marsden O, Jondeau E and Juve D 2014 An experimental characterisation of wall pressure wavevector-frequency spectra in the presence of pressure gradients *20th AIAA/CEAS Aeroacoustics Conference*
[13] Van de Wyer N, Zapata A, Nogueira D and Schram C F 2018 Development of a test rig for the measurement of turbulent boundary layer wall pressure statistics *2018 AIAA/CEAS Aeroacoustics Conference*
[14] Roger M 2017 Microphone measurements in aeroacoustic installations
[15] Corcos G M 1964 *Journal of Fluid Mechanics* **18** 353–378
[16] Raus D, Cotté B, Monchaux R, Sicard L, Jondeau E, Souchotte P and Roger M 2021 Experimental characterization of the noise generated by an airfoil oscillating above stall *AIAA AVIATION 2021 FORUM* p 2291